Tuning impurity states in bilayer graphene

Hari P. Dahal,[1,2] A. V. Balatsky,[2,3] and Jian-Xin Zhu[2,*]
[1]*Department of Physics, Boston College, Chestnut Hill, Massachusetts 02467, USA*
[2]*Theoretical Division, Los Alamos National Laboratory, Los Alamos, New Mexico 87545, USA*
[3]*Center for Integrated Nanotechnology, Los Alamos National Laboratory, Los Alamos, New Mexico 87545, USA*
(Received 7 November 2007; revised manuscript received 12 February 2008; published 12 March 2008)

We study the impurity states in bilayer graphene in the unitary limit using Green's function method. Unlike in single layer graphene, the presence of impurities at two nonequivalent sites in bilayer graphene produces different impurity states, which is understood as the change in the band structure due to interlayer hopping of electrons. The impurity states can also be tuned by changing the band structure of bilayer grahene through external electric-field bias.

DOI: 10.1103/PhysRevB.77.115114 PACS number(s): 81.05.Uw, 71.55.−i, 71.20.−b, 68.37.Ef

I. INTRODUCTION

In recent years, the fabrication of few layer graphene systems[1–3] has attracted a lot of attention to study the electronic properties of these systems. The electrons in single layer graphene show some unconventional electronic properties such as the half-integer quantum Hall effect[2] (QHE) and Klein paradox.[4] The electrons in bilayer systems also show some interesting properties as seen in QHE.[3] Many properties of the single and bilayer graphenes, such as the QHE, the possibilities of ferromagnetic transition,[5,6] and the charge inhomogeneity,[7,8] differ because of their different crystal structures. In this paper we present a systematic study of impurity effects in bilayer graphene and contrast it with that in the single layer counterpart.

The fundamental difference between single and bilayer graphenes originates from their crystal structure. Single layer graphene is an atomically thin two-dimensional hexagonal packing of sp^2 bonded carbon atoms. It is the building block of (multilayer) graphene. One unit cell of single layer graphene has two nonequivalent lattice sites (A and B). As a result, the electron wave function is spinorlike, where the sublattice index plays the role of pseudospin. The tight-binding calculation[9–11] shows that the electrons in single layer graphene disperse linearly, i.e., $E_k = \pm v_F k$, where $v_F = \frac{3ta}{2} = 5.8$ eV Å is the Fermi velocity, $t = 3.0$ eV is the nearest-neighbor hopping energy in the plane, and a is the lattice constant, and hence, are called the massless Dirac fermions. The bilayer graphene, as shown schematically in Fig. 1, can be thought of as a stacking of two identical single layer graphenes in the third dimension. In one of the common ways of layer stacking, known as Bernal stacking, only one of the nonequivalent lattice sites (site A) stays on top of another; another site (B) lies in the middle of the hexagon of the other layer.[12] The electron can hop between the layers along the bonding of these two A sites with a hopping energy ($t_\perp$), which is about ten times smaller than the hopping energy along the plane. This interlayer hopping hybridizes the p_z orbital of the carbon atom at site A, resulting in different dispersion relations of the electrons, ($E_k = \pm \frac{t_\perp}{2} \pm \sqrt{\frac{t_\perp^2}{4} + v_F^2 k^2}$).[12–14] Two of the branches of the electronic band touch each other at the Fermi energy, whereas the other two branches become gapped with an energy gap equal to $t_\perp$. The dispersion relation of the electrons corresponding to the gapless branches can be expressed in parabolic form at low momenta. The electron energy in this case has a parabolic dispersion at low momenta. In addition to this difference of the band structure between single and bilayer graphenes, the bilayer system gives the freedom of tailoring the band structure by applying an external electric-field bias (V) on the two layers. The dispersion relation in the presence of the external field bias becomes[14,15]

$$E_K = \pm \sqrt{\frac{V^2}{4} + \frac{t_\perp^2}{2} + v_F^2 k^2 \pm \sqrt{\frac{t_\perp^4}{4} + (V^2 + t_\perp^2) v_F^2 k^2}}, \quad (1)$$

which shows that the two valence (conduction) bands shift below (above) the Fermi energy by $V/2$.

To understand the electronic property of these systems, it is important to study the revealing impurity effects. The impurity states in single layer graphene have been studied by Wehling *et al.*[16] and by Bena.[17] It has been shown that if an impurity is introduced on a lattice site, a virtually bound impurity resonance state can be induced, which can be seen as an enhancement of the local density of states (LDOS) at the neighboring site. This effect is symmetric with respect to the sublattice that the impurity is on, i.e., an impurity at site B shows exactly the same effect as it is at site A. In bilayer graphene, due to the bonding between sites A of the two layers, sites A and B in each layer are no longer equivalent. The interlayer hopping distinctly differentiates the two sites. So we expect to see different impurity states with respect to

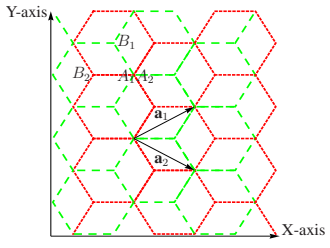

FIG. 1. (Color online) Lattice structure of bilayer graphene under consideration for a tight-binding calculation. The green (dashed) line forms the top layer and the red (dotted) line forms the bottom layer.

the location of the impurity. In addition, it is natural to expect that the external bias which changes the band structure also modifies the properties of the impurity states. This motivates us to study the impurity states in bilayer graphene as a function of both $t_\perp$ and V. The impurity effect in single layer graphene is contained in our discussion as a special case of bilayer graphene where $t_\perp=0$.

The outline of the paper is as follows: In Sec. II, we present a Green's function method to study the impurity effects. For the clean system, the results from the Green's function method is benchmarked with the exact diagonalization. In Sec. III, we present a systematic set of results and discussions. We summarize the important results in Sec. IV, and the concluding remarks are given in Sec. V.

II. THEORETICAL METHOD

In this section, we describe the theoretical method used to calculated the LDOS in the bilayer graphene using Green's function. We need to find the form of the Hamiltonian to define the free particle Green's function. The Green's function in the presence of the impurity potential is obtained by using Dyson's equation. We derive a tight-binding Hamiltonian using the lattice structure of the bilayer graphene as shown in Fig. 1. The basis vectors are chosen to be $a_1=\left(\frac{3a}{2},\frac{-\sqrt{3}a}{2}\right)$ and $a_2=\left(\frac{3a}{2},\frac{\sqrt{3}a}{2}\right)$. The corresponding basis vectors of the reciprocal space are given by $b_1=\left(\frac{2\pi}{3a},\frac{-2\pi}{\sqrt{3}a}\right)$ and $b_2=\left(\frac{2\pi}{3a},\frac{2\pi}{\sqrt{3}a}\right)$. Sites A_1 and A_2 are connected along the z direction; the electrons have $t_\perp$ hopping energy in this direction. We have assumed that the layer which has lattice sites A_1 and B_1 is biased with $V/2$, and the layer which has lattice sites A_2 and B_2 with $-V/2$ so that the potential difference between the two layers is V. For the convenience of discussion, these two layers are called the top and bottom layers, respectively.

The tight-binding equations for this lattice structure in the clean case can be written as

$$\hat{H}_{\mathbf{k}}\begin{pmatrix}\phi_{A_1}\\ \phi_{B_1}\\ \phi_{A_2}\\ \phi_{B_2}\end{pmatrix}=\varepsilon_n\begin{pmatrix}\phi_{A_1}\\ \phi_{B_1}\\ \phi_{A_2}\\ \phi_{B_2}\end{pmatrix}. \tag{2}$$

Here,

$$\hat{H}_{\mathbf{k}}=\begin{pmatrix}V/2 & \tilde{t} & -t_\perp & 0\\ \tilde{t}^* & V/2 & 0 & 0\\ -t_\perp & 0 & -V/2 & \tilde{t}^*\\ 0 & 0 & \tilde{t} & -V/2\end{pmatrix}, \tag{3}$$

with $\tilde{t}=-t\left[2\exp\left(\frac{-ik_xa}{2}\right)\cos\left(\frac{k_ya\sqrt{3}}{2}\right)+\exp(ik_xa)\right]$ and $\tilde{t}^*$ is the complex conjugate of $\tilde{t}$.

The Green's function corresponding to this Hamiltonian can be expressed as

$$\hat{G}^{(0)}(\mathbf{k},\omega)=[\omega\hat{1}-\hat{H}_{\mathbf{k}}]^{-1}, \tag{4}$$

where $\hat{1}$ represents the unit matrix. As long as all introduced impurities (up to four) are located within a single cell, we can express the local Green's function exactly through the T-matrix method, which leads to

$$\hat{G}_{ij}(\omega)=\hat{G}^{(0)}_{ij}(\omega)+\hat{G}^{(0)}_{i0}(\omega)\hat{T}(\omega)G^0_{0j}(\omega). \tag{5}$$

Here, the T matrix $\hat{T}(\omega)=\hat{U}[1-G^{(0)}(\omega)\hat{U}]^{-1}$, the local Green's function $\hat{G}^{(0)}_{ij}(\omega)=\frac{1}{N}\Sigma_{\mathbf{k}}\hat{G}^{(0)}(\mathbf{k},\omega)\exp(i\mathbf{k}\cdot\mathbf{r}_{ij})$, where the summation is over the first Brillouin zone, and $\hat{U}$ is the matrix representation of the impurity potential. The local density of states at different sites is given by $N_{A1}=\frac{-1}{\pi}G_{11}(\omega+i\gamma)$, $N_{B1}=\frac{-1}{\pi}G_{22}(\omega+i\gamma)$, $N_{A2}=\frac{-1}{\pi}G_{33}(\omega+i\gamma)$, $N_{B2}=\frac{-1}{\pi}G_{44}(\omega+i\gamma)$, where γ is the lifetime broadening. For numerical calculation, all relevant energies are measured in terms of the intralayer hopping energy of the electron, t. For simplicity, we use the impurity potential close to the unitary limit, $U=100$. The number of 1024×1024 $\mathbf{k}$ points are used in the Brillouin zone. The intrinsic lifetime broadening of $\gamma=0.005$ is taken. When we present results, unless otherwise stated, (a)–(d) represent the LDOS at sites A_1, B_1, A_2, and B_2, respectively. In each figure, the density of states (DOS) is plotted (along the vertical axis) as a function of energy E (along the horizontal axis).

We can also calculate the DOS in the absence of impurities using eigenvalues and eigenvectors of the Hamiltonian matrix [Eq. (3)]. A little algebra yields the eigenvalues

$$\varepsilon_n=\mp\sqrt{\frac{V^2}{4}+\frac{t_\perp^2}{2}+\tilde{t}\tilde{t}^*\mp\sqrt{\frac{t_\perp^4}{4}+(V^2+t_\perp^2)\tilde{t}\tilde{t}^*}}, \tag{6}$$

where ε_n represents the four eigenvalues. Note that the linearization of Eq. (6) near the corner of the Brillouin zone reduces to Eq. (1).

The corresponding eigenvectors are given by the general equation

$$\begin{pmatrix}\phi_{A1,\varepsilon_n}\\ \phi_{B1,\varepsilon_n}\\ \phi_{A2,\varepsilon_n}\\ \phi_{B2,\varepsilon_n}\end{pmatrix}=\begin{pmatrix}|\tilde{t}|^2-\left(\frac{V}{2}+\varepsilon_n\right)^2\\ |\tilde{t}|^2\left(\varepsilon_n-\frac{V}{2}\right)+\left(\frac{V}{2}+\varepsilon_n\right)\left(t_\perp^2+\frac{V^2}{4}-{\varepsilon_n}^2\right)\\ \frac{\frac{V}{2}+\varepsilon_n}{\tilde{t}}\\ 1\end{pmatrix}, \tag{7}$$

where substituting four different values of ε_n gives the four sets of eigenvectors. We normalize thus obtained 4×4 matrix of the eigenvectors and calculate the density of states on four nonequivalent sites using the standard equation

$$N_{\alpha\beta}(E)=\frac{1}{N\pi}\sum_{\mathbf{k},\varepsilon_n}|\phi_{\alpha\beta,\varepsilon_n}(\mathbf{k})|^2\left[\frac{\gamma}{(E-\varepsilon_n)^2+\gamma^2}\right], \tag{8}$$

where $\alpha=A$ and B, $\beta=1$ and 2, and $\phi_{\alpha\beta,\varepsilon_n}(\mathbf{k})$ is the normalized eigenvector. We used this DOS to check the result obtained by the Green's function method in the absence of impurity.

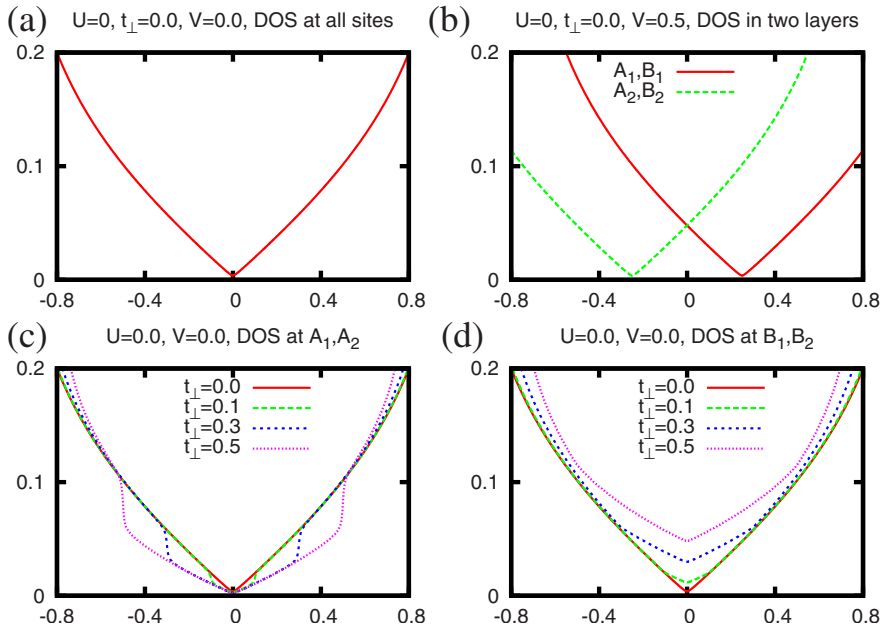

FIG. 2. (Color online) The density of states as a function of energy is shown. (a) For $t_\perp=0$, the DOS at all sites is the same and vanishes linearly at the Fermi energy. (b) For $t_\perp=0$ and $V\neq 0$, the DOS curve for sites on the top (bottom) layer shifts above (below) the Fermi energy by $V/2$, creating a finite DOS at the Fermi level. (c) For $t_\perp\neq 0$, DOS at A sites of both layers is the same, and for $-t_\perp<E<t_\perp$, it decreases compared to the single layer case. (d) DOS at sites B of both layers is the same, and for $-t_\perp<E<t_\perp$, it increases compared to the single layer case.

III. RESULTS AND DISCUSSIONS

A. Clean limit

Before getting into the discussion of the impurity states, we first discuss the effects of V and $t_\perp$ on the DOS in the absence of impurity. For $V=0$ and $t_\perp=0$, the DOS at every site is the same and it vanishes linearly in E close to the Fermi energy, as shown in Fig. 2(a). For $t_\perp=0$ but $V\neq 0$, the DOSs in the two layers are different. The overall variation of the DOS is still preserved, but the DOS curve of the upper (lower) layer shifts toward the positive (negative) energy region by $V/2$ [Fig. 2(b)]. So, the minima in the DOS for the upper (lower) layer lies at $E=|V|/2$. This results in a finite density of states at the Fermi energy. The shift in the position of the DOS minima will have a nontrivial influence on impurity states as discussed below.

The difference in the DOS of single and bilayer graphenes can be studied by using a finite value of $t_\perp$. In Figs. 2(c) and 2(d), we show the DOS at four sites for various values of $t_\perp$ but fixed $V=0$. The DOSs at A_1 and A_2 are equal and, similarly, the DOSs at B_1 and B_2 are equal but those at sites A and B are not equal in the energy range $-t_\perp<E<t_\perp$. In this energy range, the DOS at A sites is smaller than that at B sites. In particular, at the Fermi energy, the DOS at B sites is finite, but that at A sites is zero. These effects can be understood in terms of the difference in the band structure caused by a finite $t_\perp$. The band structure corresponding to sites A_1 and A_2 describes the antibonding states characterized by band gaps of $\pm t_\perp$, which results in the decreased density of states compared to that of the single layer graphene, where corresponding bands are gapless. On the other hand, the band structure corresponding to sites B_1 and B_2 is gapless at the Fermi energy and has a flatter band compared to the single layer case, resulting in a finite density of states at the Fermi level. An interesting point is that the DOS at B sites is also linear even though the dispersion relation of the electron corresponding to B sites can be approximated by a parabolic dispersion at low momenta.

Here, we also discuss the combined effect of bias and interlayer hopping on the DOS. In Figs. 3(a)–3(d), we have shown the DOS at four sites for fixed $t_\perp=0.1$ and different V. In Figs. 3(e) and 3(f), we have also shown the DOS at A_1 and B_1 for fixed $V=0.5$ and different $t_\perp$. Some additional features are seen in these figures. The DOS at all sites gets modified compared to the unbiased case [cf. Figs. 2(c) and 2(d)]. There is a shift of the DOS minimum to $E=\pm V/2$ compared to the $V=0$ case. There is also a gap opening around the Fermi energy, which increases with the increase in $t_\perp$. These unique features of band structure will lead to nontrivial impurity states.

B. Impurity states

We now discuss a single impurity in the absence of the external bias. First, we put an impurity at A_1 and study the DOS for various values of $t_\perp$. The result of the actual calculation is shown in Fig. 4. The impurity has the following effects: The DOS at the impurity site, A_1, decreases sharply. The DOS at site B_1 increases sharply, which is the signature of a virtually bound impurity resonance state. The position of the resonance peak shifts slightly below the Fermi energy with the increase in $t_\perp$. This shift of the resonance peak is

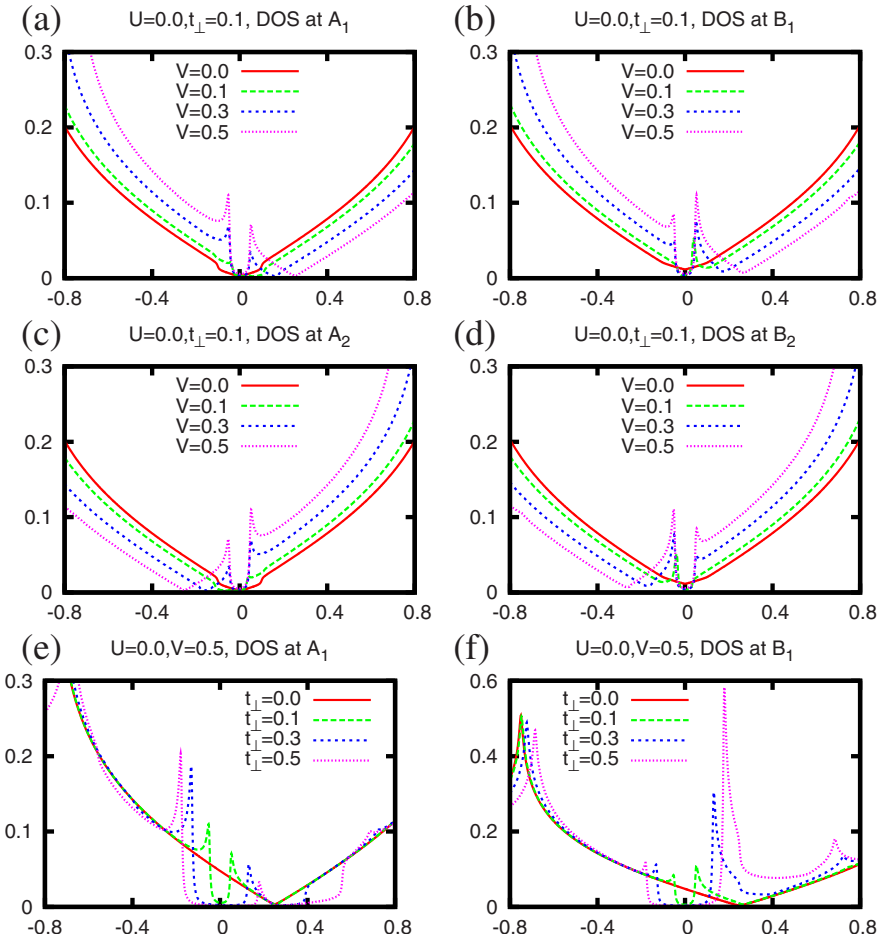

FIG. 3. (Color online) LDOS in the absence of impurity at fixed $t_\perp=0.1$ and different V. The minimum of the DOS is at $|V|/2$. Small enhancement of the DOS occurs close to the Fermi energy with the increase in V. We will show later that the position of this enhancement depends on $t_\perp$. There is a rearrangement of DOS between A and B sites. [(e) and (f)] LDOS at sites A_1 and B_1 (respectively) at fixed $V=0.5$ and different $t_\perp$ is shown. We see a gap opening around the Fermi energy. The magnitude of the gap increases with the increase in $t_\perp$. LDOS at sites A_2 and B_2 can be obtained by mirror inversion to the curves in (e) and (f) about the axis of $E=0$, respectively.

expected because the $t_\perp$ also affects the pole of the Green's function as determined by the band structure. The width of the resonance peak decreases with $t_\perp$. This is expected because the increase in $t_\perp$ depresses the band DOS on site A_1, which suppresses the scattering rate from the generated impurity state. It corresponds to an increase of lifetime, signifying a sharp resonance.

The effect on the DOS at A_2 due to the impurity at A_1 is very small. The overall behavior of the DOS curve does not change, as shown in Fig. 4(c). We see a finite DOS at A_2 at the Fermi energy, which is nothing but the finite size effect, which is not seen in Fig. 2(c) because of the extended scale used to show the DOS. When we zoom in and compare Figs. 2(c) and 4(c), we see a small enhancement in the DOS at site A_2 in the presence of an impurity at A_1 (except for $t_\perp=0$). We see some additional features in the DOS at B_2, namely, the dip-hump structure in the DOS close to the Fermi energy. We believe that the small change in the DOS at A_2 and B_2 is due to the Friedel oscillation in the bottom layer created due to the impurity at the top layer. The strength of the Friedel oscillation in the bottom layer is very small because of the geometry effect.

Now we turn to a discussion on the DOS when the impurity is at site B_1 (Fig. 5). We find that the DOS at site B_1 is sharply reduced. At all other sites, the DOS increases compared to the clean case, which is different from the result of the single impurity at the A_1 case. The DOS at A_1 increases sharply, which signifies the virtual bound state due to the impurity resonance. We notice that the height of the resonance peak at site A_1 decreases with the increase in $t_\perp$. Simultaneously, the resonance becomes broader. This effect is just opposite to the effect seen in the case when the impurity is at site A_1. This effect can be understood in terms of the band structure corresponding to site B. The increase in $t_\perp$ enhances the band DOS on site B_1, which increases the scattering rate from the generated impurity state. It corresponds to a decrease of lifetime, signifying a broader resonance. There is very little change in the overall behavior of the DOS at site A_2 compared to the no impurity case [Fig. 2(c)]. At site B_2, we see some additional features, namely, the dip-hump structure. Compared to the similar effect seen at B_2 due to the impurity at site A_1, the structure of the DOS in the present case is weaker. It is because the effect gets communicated to site B_2 through A_1 and A_2, which will be weaker

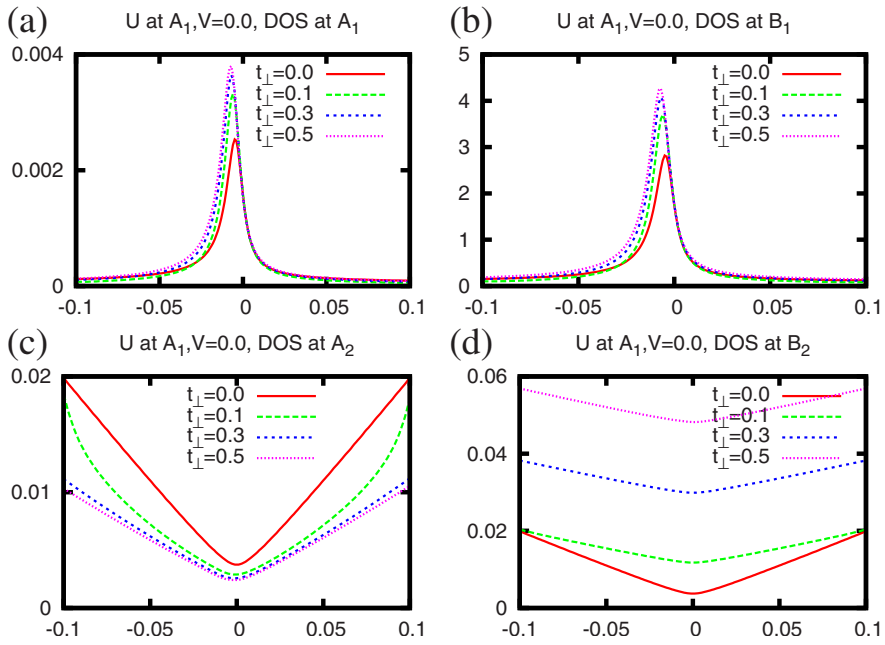

FIG. 4. (Color online) For a single impurity at site A_1, DOS as a function of energy is shown. DOS at the impurity site, A_1, is very small. DOS at the neighboring site in the same layer, B_1, is very high, which is the signature of the impurity resonance. The resonance is close to the Fermi energy. Qualitatively, the DOS at site A_2 is similar to that in the nonimpurity case [Fig. 2(c)], but it changes at site B_2. There is a small oscillation in the DOS close to the Fermi energy at site B_2.

than the previous case where the effect was communicated through only one bonding length.

Having discussed the effect in the single impurity case, it is much easier to understand the double impurity case. When there are two impurities at sites A_1 and A_2, the impurity resonance occurs at sites B_1 and B_2. The DOS at B_1 and B_2 are identical. The height of the resonance peak increases with the increase in $t_\perp$ and the resonance becomes sharper and sharper. When there are two impurities at sites B_1 and B_2, the impurity resonance occurs at sites A_1 and A_2. The DOSs at

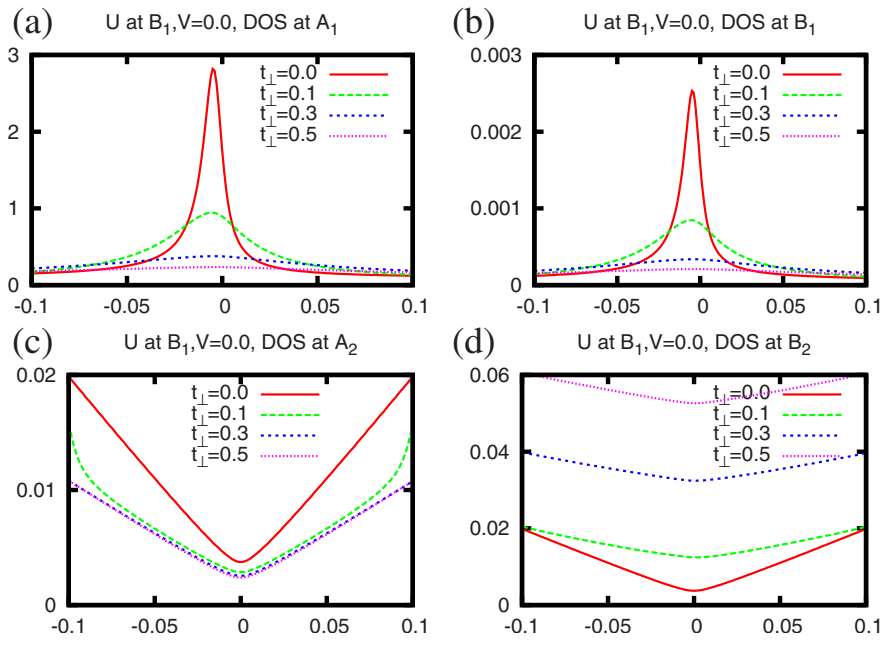

FIG. 5. (Color online) For a single impurity at site B_1, DOS as a function of energy is shown. DOS at the impurity site, B_1, is very small. DOS at the neighboring site in the same layer, A_1, is very high, which is the signature of the impurity resonance. The resonance is close to the Fermi energy. Qualitatively, the DOS at site A_2 is similar to that in the nonimpurity case [Fig. 2(c)], but it changes at site B_2. There is a small oscillation in the DOS close to the Fermi energy at site B_2.

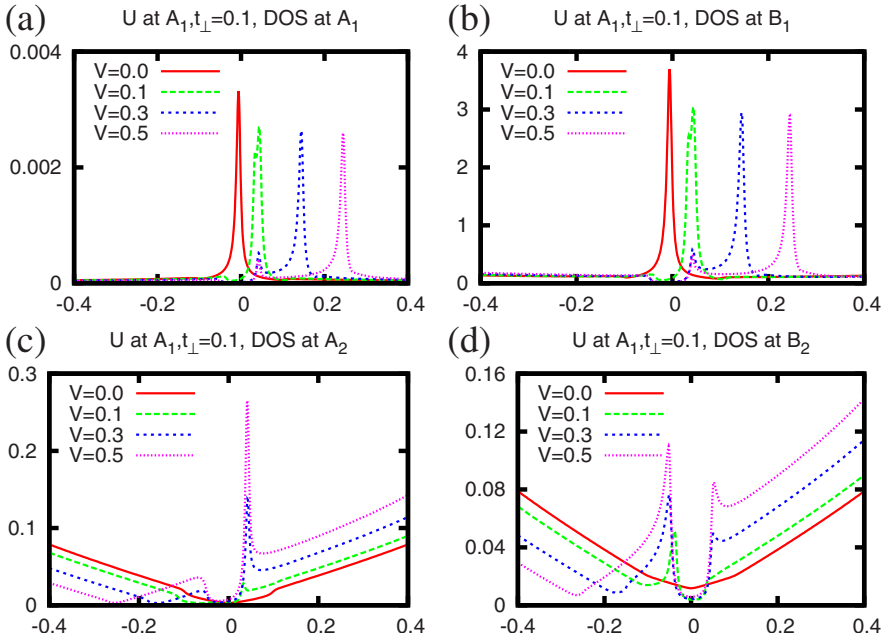

FIG. 6. (Color online) LDOS for a single impurity at site A_1 with $t_\perp=0.1$ fixed for different values of V. There is impurity resonance at site B_1. The impurity resonance is at $E=V/2$. We also see an enhancement of the DOS at site A_2 assisted by the presence of an impurity at A_1. We also see an insignificant change in DOS at site B_2.

A_1 and A_2 are identical. The height of the resonance peak decreases with the increase in $t_\perp$ and the peak width becomes broader.

Now we proceed to discuss the effect of bias on the impurity states in bilayer graphene. When there is a single impurity at site A_1, we see impurity resonance at site B_1 [Fig. 6(b)]. The position of the resonance moves above the Fermi energy by $V/2$. The height of the resonance decreases slightly with the increase in V. We also see a small satellite peak near the Fermi energy. At site A_2, we also see an impurity assisted enhancement in the DOS on the gap edge [cf. Fig. 3(c)]. At site B_2, the DOS does not show much qualitative change.

To better understand the results, especially the satellite peak of Fig. 6(b) and the position of the enhancement peak of Figs. 6(c) and 6(d), we study the change in LDOS due to change in $t_\perp$ for fixed $V=0.5$. The result is shown in Fig. 7. We find some additional information from this calculation. The strength of the satellite peak, seen in the DOS at B_1, grows with $t_\perp$. We find that the position of the peak is determined by both V and $t_\perp$. The calculation shows that the position of the satellite peak is at $E_g=\frac{V}{2}\left[\frac{t_\perp^2}{t_\perp^2+V^2}\right]^2$. This is equal to the energy gap of the second dip in the dispersion relation of the bilayer graphene in the presence of the external bias. The edge of the band gap seen in Fig. 3 is also at $E=E_g$. A similar behavior is seen at site A_2. The enhancement of the DOS seen in Fig. 6(c) for $V=0.5$ increases with $t_\perp$. The position of the peak also moves away from the Fermi energy by E_g. At site B_2, additional features are seen. The height of the small satellite peak increases with $t_\perp$. The position of the peak also shifts symmetrically above and below the Fermi level by E_g. With the increase in $t_\perp$, a clear sign of the gap opening is seen around the Fermi energy.

When there is a single impurity at site B_1 (see Fig. 8), we see different features than when there is an impurity at A_1. At $V=0$, there is a single impurity resonance close to the Fermi energy. When there is an external bias, the resonance peak at site A_1 splits into two peaks. One of the peak lies at $E=V/2$ above the Fermi energy; the other remains close to the Fermi energy. With the increase in V, the intensity of the peak at $V/2$ increases and that close to the Fermi energy decreases. At sites A_2 and B_2, we see an impurity assisted enhanced DOS close to the Fermi energy.

To better understand the result presented in Fig. 8, we perform another calculation for LDOS at fixed $V=0.5$ and different $t_\perp$. The result is shown in Fig. 9. In Fig. 9(a), we can see that the weight of LDOS at $E=V/2$ decreases with $t_\perp$. This loss of weight is transferred close to the Fermi energy. This phenomenon can be understood in terms of the change in LDOS (at fixed $V=0.5$ in the absence of the impurity) due to the change in $t_\perp$, [see Figs. 3(e) and 3(f)], where we see that a finite $t_\perp$ opens up a gap around the Fermi energy and the gap becomes more and more well defined for increased $t_\perp$. This gap leads to a different resonance state around the Fermi energy in the presence of the impurity. The shift of the weight of the LDOS close to the Fermi energy at sites A_2 and B_2 can also be understood using the same logic. We can also see in Fig. 3(f) that the LDOS at site B_1 at $E=V/2$ increases with the increase in $t_\perp$, which explains the broadening effect seen in Fig. 9(a) near $E=V/2$.

When we have two impurities at A_1 and A_2, we see impurity resonances at B_1 and B_2. The position of the impurity resonance is again determined by $V/2$. Interestingly, the impurity resonance at site B_1 lies above the Fermi energy, whereas that at site B_2 is below the Fermi energy. The DOS at B_1 can be obtained by mirror reflection of the DOS at B_2 about the axis of $E=0$.

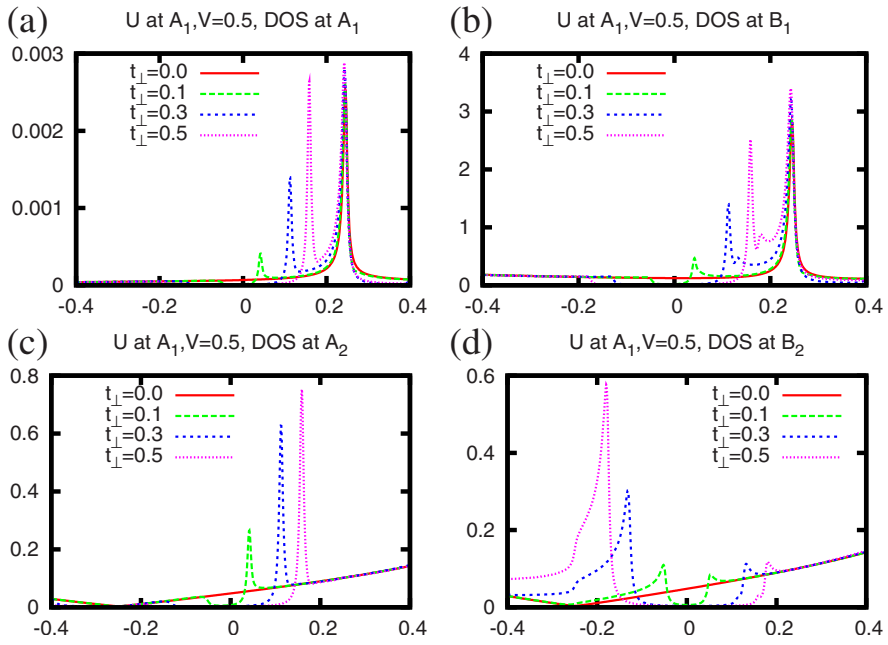

FIG. 7. (Color online) LDOS for a single impurity at site A_1, for $V=0.5$ fixed, and with the variation in $t_\perp$.

When we put two impurities at B_1 and B_2, impurity resonance arises at A_1 and A_2. The position of the impurity resonance is again determined by $V/2$. The impurity resonance at site A_1 lies above the Fermi energy, whereas that at site A_2 is below the Fermi energy. The DOS at A_1 can be obtained by mirror reflection of the DOS at A_2 about the axis of $E=0$.

IV. SUMMARY

Bilayer graphene has been created experimentally using a micromechanical cleavage method. It is always hard to obtain pristine bilayer systems experimentally. Graphene can have disorders such as cracks, unsaturated bonding, missing atoms (vacancies), foreign atoms (neutral or charged), corrugation of the surface, dislocations, and boundaries or edges. Different kinds of disorder influence the electronic properties of the system differently. The presence of disorder changes the local density of states of the clean system. Mathematically, the static disorder is modeled by adding an extra potential term in the Hamiltonian. If the disorder is local, it is modeled by a short-ranged potential. We consider a local

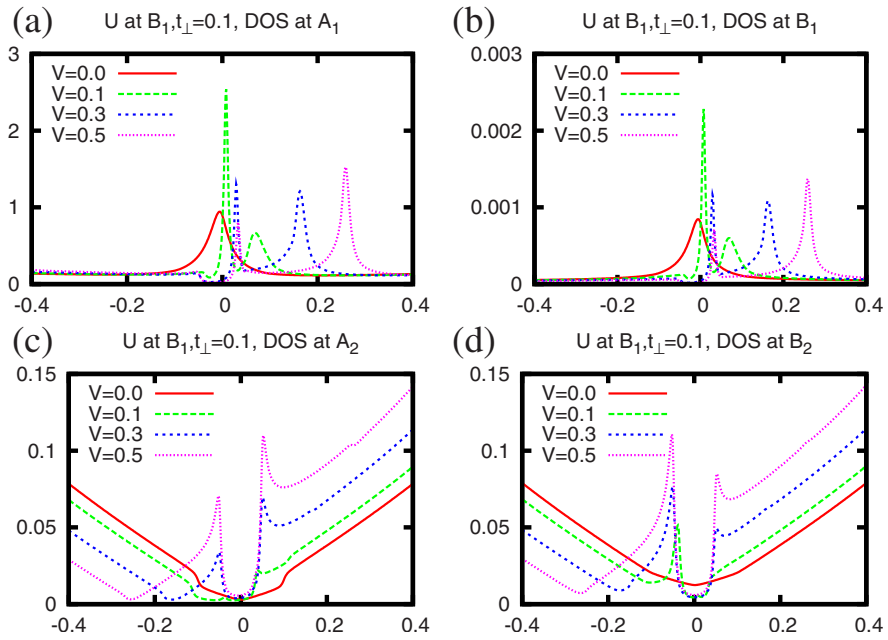

FIG. 8. (Color online) In addition to a resonance which follows $V/2$, we see some interesting features at sites A_2 and B_2.

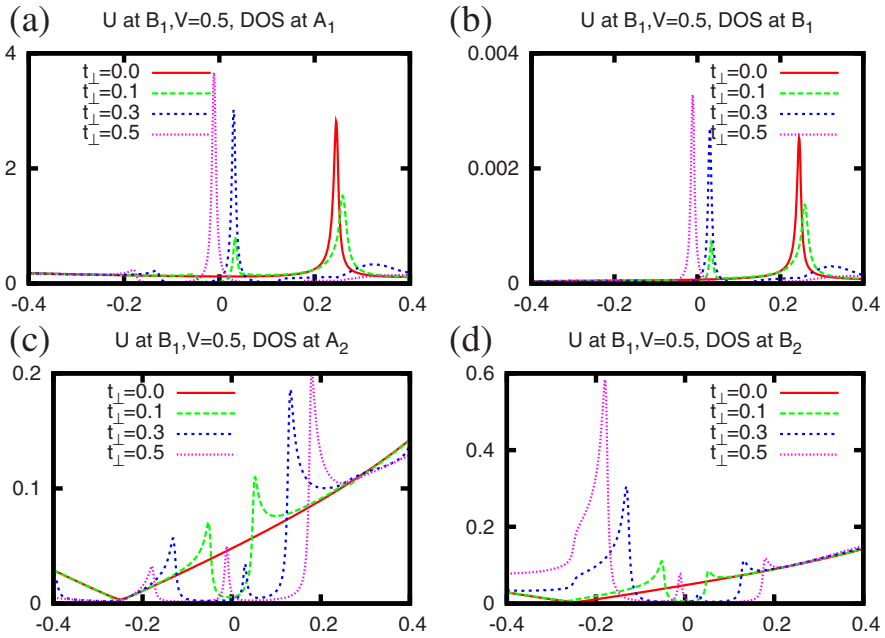

FIG. 9. (Color online) LDOS for a single impurity at site B_1 for $V=0.5$ and with the variation in $t_\perp$.

impurity produced by a missing atom (vacancy), which can be treated mathematically by introducing a contact potential in the unitary limit. For experimental purpose, a vacancy can be created by irradiating protons on the system.

We studied the impurity states in bilayer graphene for impurity potential in the unitary limit. We analyze the change in the local density of states at four lattice sites (A_1,A_2,B_1,B_2), which form the smallest unit cell of the bilayer graphene, due to the presence of impurity on one (A_1 or B_1) lattice site or two (A_1 and A_2 or B_1 and B_2) lattice sites. Here, A_1,B_1 and A_2,B_2 are the nonequivalent lattice sites of the top and bottom layers, respectively. Normally the impurity state is identified as an enhancement of the LDOS in the neighboring lattice sites of the impurity site. In bilayer graphene, two neighboring sites (A_1 and B_1) are not equivalent because only one of the sites (A_1) is connected to the lattice site (A_2) of the other layer. Therefore, electrons can hop between the two layers only along A_1A_2 (interlayer hopping). It leads to different impurity states when impurity is placed either on A_1 or on B_1 sites. This observation is different than in the single layer graphene, where the impurity state is insensitive to the lattice site on which the impurity is placed. We study the effect of the interlayer hopping on the impurity states in bilayer graphene. Furthermore, contrary to the single layer graphene, the band structure of the bilayer graphene can be changed by applying an external bias. The most significant change is on the band structure, namely, the opening of a band gap. It is probably hard to make individual contacts to the two layers of the bilayer graphene to bias them with opposite polarities because the separation of the two layers is very small (3.35 Å). However, an experiment has already been done where the theoretically predicted band gap opening due to the bias is tested successfully.[18] Thus, we study the effect of the external bias on the impurity states. Since, we have two tuning parameters, the external bias and the interlayer hopping, we also study their combined effects on the impurity states.

In the clean limit, the LDOS in the single layer graphene varies linearly with energy and vanishes at the Fermi energy. In the absence of an external bias, the LDOS at all sites of the bilayer graphene is also minimum at the Fermi energy although its magnitude is unequal for lattice sites A and B (zero at sites A_1,A_2 and finite at B_1,B_2). When the impurity is at site A_1, we find an impurity resonance at site B_1 and vice versa. The resonance state is close to the Fermi energy because the density of state has its minimum at this energy. The width of the resonance at B_1 (A_1) when the impurity is at A_1 (B_1) decreases (increases) with the increase in the interlayer hopping. Therefore, the impurity at A_1 (B_1) produces relatively long (short) lived bound states at B_1 (A_1). It is understood as the effect of the enhanced (suppressed) density of states at the B_1 (A_1) band around the Fermi energy due to the interlayer hopping. The change in the local density of states at the lattice sites of the other layer (A_2 and B_2) is small.

When the external bias is finite, we consider that the top layer is biased positively ($V/2$) and the bottom layer is biased negatively ($-V/2$) so that the net potential difference between the two layers is V. In the limit when the interlayer hopping is zero, the minimum of the density of state at A_1 and B_1 (A_2 and B_2) shifts above (below) the Fermi energy by $V/2$ ($-V/2$). It leads to the shift in the position of the impurity states above (below) the Fermi energy by $V/2$ ($-V/2$). Hence, we show that the impurity states in bilayer graphene can be tuned by using an external bias.

When both the interlayer hopping and external bias are finite, a gap opens around the Fermi energy at both A and B lattice sites. The gap is equal to $E_g=\frac{V}{2}\left[\frac{t_\perp^2}{t_\perp^2+V^2}\right]^2$. The gap increases with the interlayer hopping. For lattice site A_1, the minimum of the LDOS due to the external bias (which is above the Fermi energy at $E=V/2$) remains as it is. How-

ever, at site B_1, the LDOS at $E=V/2$ increases. We observe a different impurity state due to the presence of the impurity at A_1 or B_1. When the impurity is at A_1, two impurity resonance peaks show up in the LDOS at B_1. One is at $E=V/2$ and another at $E=E_g$. The weight of the peak at $E=E_g$ significantly increases with the interlayer hopping. When the impurity is at B_1, we still get two resonance peaks at A_1. The difference is that one resonance is at $E=V/2$ and the other is close to the Fermi energy. Furthermore, these two resonances compete when the interlayer hopping is increased. The resonance at $E=V/2$ loses its weight and becomes broader (due to the enhanced LDOS at B_1 at $E=V/2$), whereas the resonance close to the Fermi energy gains weight when the interlayer hopping is increased.

We show that very nontrivial and interesting impurity states can be created in bilayer graphene. We can tune these states by putting impurities in different lattice sites and by changing the interlayer hopping and external bias. We propose that scanning tunneling microscopy (STM) can be used to test these impurity states. STM experiments have already been successfully used in graphite,[19] carbon nanotube,[20–22] and in single and bilayer graphenes[23,24] to characterize the disorder and to determine the local density of states as a function of energy. The basic principle is that by using STM we can determine the tunneling current as a function of the bias at the lattice sites of interest. Using differential tunneling conductance, we can map out the local density of states.

Our results are correct for an idealized model of the bilayer graphene, i.e., without taking into account the effects of the electron-electron (e-e) and electron-phonon (e-ph) interactions. The inclusion of the e-e and e-ph interactions renormalizes the band structure of the bilayer graphene. Mathematically, it amounts to replacing the bare Green's function, $\hat{G}^{(0)}(\mathbf{k},\omega)$, by a dressed Green's function, $\hat{G}^{(0)}(\mathbf{k},\omega)$. Each matrix element of $\hat{G}^{(0)}(\mathbf{k},\omega)$ [see Eq. (4)] will then have an additional self-energy term as shown in Ref. 25. In reality, we know that the interaction does not significantly change the band structure of the bilayer graphene because the band structure predicted theoretically without including the e-e and e-ph interactions does not differ much from the band structure obtained experimentally in the angle resolved photoemission spectroscopy experiment (there is only a small extra kinklike feature).[26] In general, the inclusion of the interactions introduces some features in the LDOS, but the low energy enhancement of the LDOS due to the impurity in the unitary limit always exists.[25] Hence, we believe that the main features of the impurity resonance states discussed here do not change even if we consider a more practical model of the bilayer graphene.

The results are valid for a bilayer system in which two layers are stacked in a special fashion, namely, Bernal stacking. Although Bernal stacking is one of the most common ways of stacking multiple layers of graphene, the top layer of the multilayer graphene can be twisted in a two-dimensional plane. It is seen experimentally that the epitaxially grown multilayer graphene has orientation disorder.[27] The electronic properties of a bilayer graphene with a small rotation of the top layer with respect to the bottom layer are analytically studied.[28] It has been shown that the dispersion relation of the electron in such a bilayer is linear and the band structure is semimetallic. In the presence of the external bias, the band gap cannot be opened. In this case, we would need to do another calculation to precisely determine how the details of the results discussed in this paper change. However, we can make some intuitive predictions. Since the dispersion relation of the electrons looks more like that of the single layer graphene, the impurity states will also be quantitatively similar to that of the single layer graphene.

V. CONCLUDING REMARKS

Before concluding, we would like to make two comments. To our knowledge, two studies have been done which resembles our work. Wang *et al.*[29] have studied the effects of voids in the absence of external bias. In particular, they investigated the quantum interference pattern in a specific energy and no impurity induced resonance states were discussed. Similarly, the disorder problem in biased bilayer graphene was studied by Nilsson and Castro Neto.[15] In our work, we have addressed the issue about the sensitivity of the impurity induced resonance states to the underlying electronic band structure in a bilayer graphene through the application of pressure or/and electric bias, which were not discussed in these literatures.

In conclusion, we study the possibility of tuning the impurity states in a bilayer graphene. We systematically study the signature of the impurity resonance states by looking at the local density of states at four inequivalent sites of the bilayer graphene. This work is the most detailed study of the impurity states in bilayer graphene. We have shown that in bilayer graphene, the impurity states can be tuned using an external bias and changing the interlayer hopping energy. Our predictions about the evolution of the impurity states in bilayer graphene can be tested by scanning tunneling microscopy.

ACKNOWLEDGMENTS

One of us (H.D.) is grateful to K. Bedell and Boston College for financial support. This work was supported by DOE at Los Alamos under Grant No. DE-AC52-06NA25396 and the LDRD programs.

*jxzhu@lanl.gov; URL: http://theory.lanl.gov

[1] K. S. Novoselov, V. V. K. D. Jiang, T. Booth, S. M. Morozov, and A. K. Geim, Proc. Natl. Acad. Sci. U.S.A. **102**, 10451 (2005).
[2] K. S. Novoselov, A. K. Geim, S. V. Morozov, D. Jiang, M. I. Katsnelson, I. V. Grigorieva, S. V. Dubonos, and A. A. Firsov, Nature (London) **438**, 197 (2005).
[3] K. S. Novoselov, E. McCann, S. V. Morozov, V. I. Falko, M. I. Katsnelson, U. Zeitler, D. Jiang, F. Schedin, and A. K. Geim, Nat. Phys. **2**, 177 (2006).
[4] M. I. Katsnelson, K. S. Novoselov, and A. K. Geim, Nat. Phys. **2**, 620 (2006).
[5] N. M. R. Peres, F. Guinea, and A. H. Castro Neto, Phys. Rev. B **72**, 174406 (2005).
[6] J. Nilsson, A. H. Castro Neto, N. M. R. Peres, and F. Guinea, Phys. Rev. B **73**, 214418 (2006).
[7] H. P. Dahal, Y. N. Joglekar, K. S. Bedell, and A. V. Balatsky, Phys. Rev. B **74**, 233405 (2006).
[8] H. P. Dahal, T. O. Wehling, K. S. Bedell, J.-X. Zhu, and A. V. Balatsky, arXiv:0706.1689 (unpublished).
[9] P. R. Wallace, Phys. Rev. **71**, 622 (1947).
[10] G. W. Semenoff, Phys. Rev. Lett. **53**, 2449 (1984).
[11] F. D. M. Haldane, Phys. Rev. Lett. **61**, 2015 (1988).
[12] J. Nilsson, A. H. Castro Neto, F. Guinea, and N. M. R. Peres, Phys. Rev. Lett. **97**, 266801 (2006).
[13] E. McCann and V. I. Falko, Phys. Rev. Lett. **96**, 086805 (2006).
[14] E. McCann, Phys. Rev. B **74**, 161403(R) (2006).
[15] J. Nilsson and A. H. Castro Neto, Phys. Rev. Lett. **98**, 126801 (2007).
[16] T. O. Wehling, A. V. Balatsky, M. I. Katsnelson, A. I. Lichtenstein, K. Scharnberg, and R. Wiesendanger, Phys. Rev. B **75**, 125425 (2007).
[17] C. Bena, arXiv:cond-mat/0706411 (unpublished).
[18] J. B. Oostinga, H. B. Heersche, X. Liu, A. F. Morpurgo, and L. M. K. Vandersypen, Nat. Mater. **7**, 151 (2007).
[19] Y. Niimi, T. Matsui, H. Kambara, K. Tagami, M. Tsukada, and H. Fukuyama, Phys. Rev. B **73**, 085421 (2006).
[20] T. W. Odom, J.-L. Huang, and C. M. Lieber, J. Phys.: Condens. Matter **14**, R145 (2002).
[21] M. Ouyang, J.-L. Huang, C. L. Cheung, and C. M. Lieber, Science **291**, 97 (2001).
[22] Z. Osvath, G. Vertesy, L. Tapaszto, F. Weber, Z. E. Horvath, J. Gyulai, and L. P. Biro, Phys. Rev. B **72**, 045429 (2005).
[23] G. M. Rutter, J. N. Crain, N. P. Guisinger, T. Li, P. N. First, and J. A. Stroscio, Science **317**, 219 (2007).
[24] V. W. Brar, Y. Zhang, Y. Yayon, T. Ohta, J. L. McChesney, A. Bostwick, E. Rotenberg, K. Hom, and M. F. Crommie, Appl. Phys. Lett. **91**, 122102 (2007).
[25] J.-X. Zhu, Jun Sun, Qimiao Si, and A. V. Balatsky, Phys. Rev. Lett. **92**, 017002 (2004).
[26] T. Ohta, A. Bostwick, T. Seyller, K. Horn, and E. Rotenberg, Science **313**, 951 (2006).
[27] J. Hass, R. Feng, T. Li, X. Li, Z. Zong, W. A. de Heer, P. N. First, E. H. Conrad, C. A. Jeffrey, and C. Berger, Appl. Phys. Lett. **89**, 143106 (2006).
[28] J. M. B. Lopes dos Santos, N. M. R. Peres, and A. H. Castro Neto, Phys. Rev. Lett. **99**, 256802 (2007).
[29] Z. Wang, Q. Li, H. Su, X. Wang, Q. Shi, J. Chen, J. Yang, and J. Hou, Phys. Rev. B **75**, 085424 (2007).